

10-2019

## Biophysical and Biomechanical Properties of Neural Progenitor Cells as Indicators of Developmental Neurotoxicity

Gautam Mahajan  
*Cleveland State University*

Moo-Yeal Lee  
*Cleveland State University*

Chandrasekhar R. Kothapalli  
*Cleveland State University*

Follow this and additional works at: [https://engagedscholarship.csuohio.edu/encbe\\_facpub](https://engagedscholarship.csuohio.edu/encbe_facpub)

 Part of the [Biomechanics and Biotransport Commons](#), and the [Toxicology Commons](#)

**How does access to this work benefit you? Let us know!**

---

### Repository Citation

Mahajan, Gautam; Lee, Moo-Yeal; and Kothapalli, Chandrasekhar R., "Biophysical and Biomechanical Properties of Neural Progenitor Cells as Indicators of Developmental Neurotoxicity" (2019). *Chemical & Biomedical Engineering Faculty Publications*. 161.

[https://engagedscholarship.csuohio.edu/encbe\\_facpub/161](https://engagedscholarship.csuohio.edu/encbe_facpub/161)

This Article is brought to you for free and open access by the Chemical & Biomedical Engineering Department at EngagedScholarship@CSU. It has been accepted for inclusion in Chemical & Biomedical Engineering Faculty Publications by an authorized administrator of EngagedScholarship@CSU. For more information, please contact [library.es@csuohio.edu](mailto:library.es@csuohio.edu).

# Biophysical and biomechanical properties of neural progenitor cells as indicators of developmental neurotoxicity

Gautam Mahajan · Moo-Yeal Lee · Chandrasekhar Kothapalli

## Abstract

Conventional in vitro toxicity studies have focused on identifying  $IC_{50}$  and the underlying mechanisms, but how toxicants influence biophysical and biomechanical changes in human cells, especially during developmental stages, remain under-studied. Here, using an atomic force microscope, we characterized changes in biophysical (cell area, actin organization) and biomechanical (Young's modulus, force of adhesion, tether force, membrane tension, tether radius) aspects of human fetal brain-derived neural progenitor cells (NPCs) induced by four classes of widely used toxic compounds, including rotenone, digoxin, *N*-arachidonylethanolamide (AEA), and chlorpyrifos, under exposure up to 36 h. The sub-cellular mechanisms (apoptosis, mitochondria membrane potential, DNA damage, glutathione levels) by which these toxicants induced bio-chemical changes in NPCs were assessed. Results suggest a significant compromise in cell viability with increasing toxicant concentration ( $p < 0.01$ ), and biophysical and biomechanical characteristics with increasing exposure time ( $p < 0.01$ ) as well as toxicant concentration ( $p < 0.01$ ). Impairment of mitochondrial membrane potential appears to be the most sensitive mechanism of neurotoxicity for rotenone, AEA and chlorpyrifos exposure, but compromise in plasma membrane integrity for digoxin exposure. The surviving NPCs remarkably retained stemness (SOX2 expression) even at high toxicant concentrations. A negative linear correlation ( $R^2 = 0.92$ ) exists between the elastic modulus of surviving cells and the number of living cells in that environment. We propose that even subtle compromise in cell mechanics could serve as a crucial marker of developmental neurotoxicity (mechanotoxicology) and therefore should be included as part of toxicology assessment repertoire to characterize as well as predict developmental outcomes.

**Keywords** Developmental neurotoxicity · Neural stem cells · Insecticides · AEA · Chlorpyrifos · Multi-variable logistic regression · Mechanotoxicology

## Introduction

During central nervous system (CNS) development, the large reservoirs of neural progenitor cells (NPCs) in the ventricular and subventricular zones decline with maturation and aging. For instance, the large NPC population in neural crest and neural spinal tube dramatically declined to  $\leq 1\%$

postnatal in a rat embryogenesis model, highlighting the role of NPCs and their microhabitat in normal embryogenesis (Ladran et al. 2013; Rammensee et al. 2017). NPCs are self-renewing, multi-potent cells which can differentiate into neuronal and glial lineages. CNS development is a complex process comprising several highly coordinated events such as migration, differentiation, proliferation, cell death, myelination, and synthesis of neurotransmitters (Xu et al. 2017), which occur in a well-defined time-frame, making each event differentially vulnerable on exposure to harmful compounds. Any perturbation during CNS development could lead to permanent damage with little chance to repair. Epidemiological studies have detailed the role of environmental chemicals and clinical drugs on neurological disorders such as learning disabilities, lowered IQ, cognitive dysfunction, impaired verbal skills, and poor perceptual and motor skills (Lee et al. 2016; Malik et al. 2014).

Neurological insults during the first trimester could manifest during later stages of adolescence as developmental disorders, which currently affects one in every six children (Ross et al. 2015; Tamm and Ceccatelli 2017). This has prompted the need to methodically screen a range of widely known environmental and pharmaceutical compounds for their potential neurodevelopmental toxicity. Animal models have been widely used to flag compounds for toxicological identification. In the field of reproductive and developmental toxicology, higher number of experimental animals are typically used, mostly for statistical significance purposes (Bjorling-Poulsen et al. 2008). Since animal models are xenogeneic, expensive, poorly predictive of human outcomes, and ethically and morally contentious, demand for alternative in vitro test methods has been growing. In the absence of developmentally relevant fresh primary brain cells, immortalized cell lines such as embryonic stem cells (ESCs), induced pluripotent stem cells (iPSCs), primary trophoblast cells, NPCs, and primary neurons are being explored to elucidate neurotoxicity of various classes of compounds (Bal-Price et al. 2010; Ebert et al. 2012). However, current in vitro tests focus mostly on biochemical assays to assess the toxicity, while important changes in biophysical and biomechanical characteristics of these progenitor cells were rarely studied (Liu et al. 2015; Wu et al. 2012).

CNS development is a tightly regulated process, from maturation of neurons to folding of the brain, and relies heavily on mechanical forces and biochemical cues (Franze 2013). For instance, radial glial cells clonally linked to NPCs act as a mechanical scaffold for cell migration during brain formation (Barnes et al. 2017), highlighting the importance of intrinsic cellular mechanical characteristics such as membrane tension in organizing motility, cell shape, and mechanotransduction (Diz-Munoz et al. 2013). Perturbations to cellular biophysical aspects could change the coupling between cellular intrinsic forces and matrix mechanical properties, causing abnormal mechanotransduction (Kolahi and Mofrad 2010). Cell mechanics is gaining traction as an important biomarker of cell differentiation, pathophysiology, and cancer progression (Li et al. 2008; Liang et al. 2016; Liu et al. 2015; Qiu et al. 2010). The biomechanics of various cell types has been explored using optical tweezers, micropipette aspiration, magnetic twisting cytometry, and atomic force microscopy (AFM), among others (Lins et al. 2018; Pillarisetti et al. 2011; Yim et al. 2010; Yokokawa et al. 2008). The utility of AFM to study the mechanical properties of individual cells under pathological and toxicant-aberrant conditions is gaining attention (Angely et al. 2017; Gavara and Chadwick 2012; Kim et al. 2012; Pastrana et al. 2019). However, characterization of the changes in biophysical and biomechanical properties and correlation of the biomechanical and biochemical outcomes after toxicants exposure remain unexplored.

Since biochemical and biomechanical cues play an integral role in regulating fetal development (Wozniak and Chen 2009), in this work, we used human fetal NPCs to evaluate the cytotoxic potential of various classes of compounds on developmental neurotoxicity. We evaluated the sub-cellular mechanisms of action of rotenone, digoxin, chlorpyrifos, and arachidonylethanolamide (AEA) over a wide range of concentrations. These four compounds have been selected for their toxic potential in various in vitro and in vivo conditions, although the extent of their prior testing was confined to quantifying  $IC_{50}$  or  $LD_{50}$  levels (Bal-Price et al. 2010; Bjorling-Poulsen et al. 2008; Dubovicky et al. 2008; Giordano and Costa 2012; Movsesyan et al. 2004; Tamm and Ceccatelli 2017). Using AFM, we not only quantified the changes in physical and mechanical properties of NPCs treated with these compounds, but also correlated the biochemical outcomes with biomechanical characteristics of cells.

## Materials and methods

### Cell culture and compound exposure

Human NPCs (ReNcell VM; SCC008; EMD Millipore, Burlington, MA, USA) were maintained in an undifferentiated state by culturing in a complete medium (ReNcell maintenance medium; SCM005; EMD Millipore) supplemented with 20 ng/mL each of bFGF and EGF, and 1% penicillin/streptomycin, on laminin-coated flasks. Stock solutions of rotenone, digoxin, and chlorpyrifos were prepared in DMSO at 10 mM, while AEA was prepared in ethanol at 10 mM. Unless specified otherwise, all the compounds, growth factors, and solvents were purchased from Sigma-Aldrich (St. Louis, MO, USA). The working concentrations of the compounds were prepared by serial dilution of stock solutions in DMSO and followed by dilution in the complete medium.

### Cell viability measurement

ReNcell VM was cultured in 96-well tissue-culture plates at a density of  $15 \times 10^3$  cells/well and exposed to a range of concentrations of the four individual compounds for 24 h. A Live/Dead<sup>®</sup> viability/cytotoxicity kit (Thermo Fisher Scientific, Waltham, MA, USA) was used to evaluate the effect of each compound on cell survival ( $n = 4$  wells/concentration/compound) (Tasneem et al. 2016). Images of cells in individual wells were acquired using an automated fluorescent microscope (S + scanner, Samsung Eletro-Mechanics, Co. (SEMCO), South Korea). (Details in supplementary methods) (Joshi et al. 2018b).

## Assays for cellular mechanisms of toxicity

All assays were performed with an initial seeding density of  $15 \times 10^3$  cells/well. Additional details for these methods, where necessary, were provided in supplementary methods.

### DNA damage

After 24 h of compound exposure, surviving cells ( $n=4$  wells/concentration/compound) were stained with  $15 \mu\text{M}$  of Hoechst 33342 (Thermo Fisher Scientific; Ex-352 nm/Em-416 nm) in  $1 \times \text{PBS}$  (pH  $\sim 7.2$ ) for 30 min to assess changes in nucleic DNA content. Nuclei were imaged using the S + scanner with a  $4 \times$  objective and a blue fluorescence filter from Semrock (DAPI-5060C-000) (Joshi et al. 2018b).

### Mitochondrial membrane potential assay

Mitochondrial impairment, i.e., changes in mitochondrial membrane potential, in the presence of the compounds was assessed using tetramethyl rhodamine methyl ester (TMRM; Thermo Fisher Scientific; Ex-545 nm/Em-600 nm). The cells were stained with  $0.5 \mu\text{M}$  of TMRM after 24 h of compound exposure and imaged using the S + scanner with a  $4 \times$  objective and an orange filter from Semrock (TxRed-4040C-000) (Joshi et al. 2018b).

### YO-PRO<sup>®</sup>-1 assay to identify apoptotic cells

YO-PRO<sup>®</sup>-1 (Thermo Fisher Scientific; Ex-491 nm/Em-509 nm) identifies apoptotic cells via nucleic acid binding. Apoptotic cells are permeant to YO-PRO<sup>®</sup>-1, but non-permeant to propidium iodide which could stain only dead cells. After 24 h of compound exposure, live cells ( $n=4$  wells/concentration/compound) were incubated with  $5 \mu\text{M}$  of YO-PRO<sup>®</sup>-1 for 30 min. Using a Zeiss Axio Vert. A1 inverted fluorescence microscope (Thornwood, NY, USA), at least 10 images were taken at random locations in each well. The fold change in number of apoptotic cells in toxicant exposed cases was calculated by normalizing it to controls.

### Intracellular glutathione levels

ReNcell VM ( $n=4$  wells/concentration/compound) was stained with  $50 \mu\text{M}$  of monochlorobimane (mBCI; Thermo Fisher Scientific; Ex-394 nm/Em-490 nm) after 24 h compound exposure to determine the levels of intracellular glutathione (GSH), which provides an indirect measure of cellular defense against oxidative stress. Lower GSH levels are associated with increased concentrations of glutathione disulfide (GSSG) leading to a decrease in GSH/GSSG ratio, a critical indicator of cellular health. The cells were imaged

at  $4 \times$  magnification using the S + scanner with the blue filter (Joshi et al. 2018b).

## Biophysical and biomechanical measurements using AFM

ReNcell VM at a seeding density of  $1.5 \times 10^5$  cells was cultured in laminin-coated 50 mm AFM-specific petri dishes for 24 h and exposed to compounds for up to 36 h. All measurements were made using a MFP-3D-Bio atomic force microscope (AFM; Oxford Instruments, Santa Barbara, CA, USA) mounted on an inverted fluorescence microscope (Nikon Eclipse Ti; Melville, NY, USA). Tip-less AFM cantilevers (Arrow<sup>™</sup> TL1, Nanoworld, nominal spring constant-0.03 N/m) were modified by attaching a  $4.5\text{-}\mu\text{m}$  polystyrene bead using epoxy as explained earlier (Joshi et al. 2018a). The cells were maintained at  $37^\circ\text{C}$  throughout the live-cell nanoindentation assay. For each experiment, 50–60 cells were randomly selected, and force curves were obtained between nucleus and cell margin at approach/retraction velocity of  $5 \mu\text{m/s}$ . At least 60 force-indentation curves were obtained for each group of the cells (controls and compound-treated; 4, 12, 24, and 36 h). Using Hertz's contact model, the Young's modulus was determined from the force-indentation curves as  $F = 4E_Y \sqrt{R\delta^3/3(1-\mu^2)}$ , where  $F$  is indentation force,  $E_Y$  is Young's modulus,  $\mu$  is Poisson's ratio (0.5 for cells),  $R$  is tip radius ( $2.25 \mu\text{m}$ ) and  $\delta$  is indentation depth ( $\sim 500 \text{ nm}$ ). The force required to separate AFM tip and cell surface describes the adhesion or force of adhesion ( $F_{ad}$ ). The tether forces ( $F_T$ ) were directly calculated from the series of force steps in the retraction curve. The average noise of  $50 \text{ pN}$  was set as a threshold of tether force and only forces higher than threshold was considered as actual rupture events. The apparent membrane tension ( $T_M$ ), the force needed to deform a membrane, was calculated from tether forces using  $T_M \approx F_T^2/8\pi^2 K_B$ , where  $K_B$  is the bending stiffness which lies in the range of  $0.1\text{--}0.3 \text{ pN}\cdot\mu\text{m}$  (Diz-Munoz et al. 2013; Diz-Munoz et al. 2010; Hochmuth et al. 1996). Similarly,  $R_T$  (tether radius), which describes the connection between plasma membrane and cytoskeleton, was calculated from the tether forces as  $R_T \approx 2\pi K_B/F_T$  (additional details in Supplementary Methods).

### SOX2 staining for undifferentiated ReNcell VM

After 24 h of compound exposure, ReNcell VM was washed twice with  $1 \times \text{PBS}$ , fixed with 4% paraformaldehyde for 30 min, washed twice with  $1 \times \text{PBS}$  for 5 min each, and incubated with a permeabilizing/blocking buffer solution containing 5% goat serum and 0.5% Triton-X in PBS for 30 min. After removing the permeabilizing/blocking buffer solution, the cells were incubated with mouse monoclonal anti-SOX2 (Thermo Fisher Scientific) for 4 h. The cells

were washed twice with 1×PBS and incubated with goat anti-mouse FITC secondary antibody (1:100; Santa Cruz Biotechnology) for 2 h at room temperature. The cells were washed twice with PBS, incubated with DAPI for 10 min, and washed once with PBS before imaging. At least five images were taken at random locations in each well using a 10× objective on the inverted fluorescence microscope (Zeiss Axio Vert A1).

### Actin staining

After 4, 12, 24, and 36 h of compound exposure, ReNcell VM was washed once with 1×PBS, fixed with 4% PFA for 40 min, washed twice with PBS for 5 min, and incubated with 0.1% Triton X-100 in PBS for 5 min. The cells were washed twice with PBS and incubated with actin-staining Alexa Flour 488 Phalloidin (Thermo Fisher Scientific) for 25 min at room temperature. After removing the staining solution, the cells were washed twice with PBS for 5 min and incubated with DAPI for 10 min before imaging. Images were taken at random locations using a 20× objective on the inverted fluorescence microscope. The images were used to calculate changes in cell area using ImageJ.

### Statistical analysis

Data were represented as mean ± standard error from at least  $n=4$  wells/condition, with at least three independent repeats of each assay, and statistical analysis was performed using GraphPad Prism 5. Data analysis was performed using one-way and two-way ANOVA, based on the number of groups compared, followed by Tukey multiple comparison or Bonferroni post hoc test, to find statistically significant differences between the groups.  $p < 0.05$  deemed statistically significant. Multivariate logistic regression of the parameters contributing to NPC health was performed using R software (version 3.5.2).

## Results

### Biochemical and biomechanical effects of rotenone exposure

To investigate the cytotoxic potential of rotenone on human NPCs, ReNcell VM was exposed to a range of rotenone concentrations (0.1–25 μM) for 24 h. A dose-dependent decrease in cell viability was observed with a calculated  $IC_{50}$  value of  $0.27 \pm 0.01$  μM (Fig. 1a). To elucidate the subcellular mechanisms of rotenone toxicity, damage to nucleic DNA ( $IC_{50} \cong 0.28 \pm 0.01$  μM) and mitochondria ( $IC_{50} \cong 0.22 \pm 0.01$  μM), as well as changes in glutathione levels ( $IC_{50} \cong 0.33 \pm 0.02$  μM) were assessed (Fig. 1b). An

increase in the number of apoptotic cells by YO-PRO<sup>®</sup>-1 staining was noted at  $\leq 0.78$  μM concentration, beyond which necrosis might be dominating the mechanism of cell death (Fig. 1c). Based on these  $IC_{50}$  values, mitochondrial impairment seems to be the dominant mechanism by which rotenone influences a compromise in NPC health ( $p < 0.01$  vs. other mechanisms; Supplementary Figure 3). However, no significant changes in SOX2 expression were noted in the surviving and adherent ReNcell VM upon rotenone exposure (Supplementary Figure 1).

No significant changes in the biophysical and biomechanical characteristics ( $E_Y$ ,  $F_{ad}$ ,  $F_T$ ) of ReNcell VM were noted in control cultures at 4, 12, 24 and 36 h time points (Supplementary Figure 2). The baseline properties of control ReNcell VM were:  $E_Y = 5.04 \pm 0.16$  kPa,  $F_{ad} = 2.47 \pm 0.03$  nN,  $F_T = 329 \pm 3.2$  pN,  $T_M = 13.9 \pm 0.27$  pN/μm, and  $R_T = 1.9 \pm 0.01$  nm. The mechanical properties of control ReNcell VM at the 24-h time point were used as a reference vs. test cases. Significant decreases in  $E_Y$ ,  $F_{ad}$ ,  $F_T$ , and  $T_M$  with concomitant increases in  $R_T$  were noted, as a function of increasing exposure duration ( $p < 0.001$  vs. controls) and toxicant concentration ( $p < 0.001$  vs. controls) in ReNcell VM exposed to rotenone (Fig. 1d–h). Significant concentration-dependent differences in biomechanical and biophysical characteristics of ReNcell VM were noted at every time point, while such differences were more pronounced at higher concentrations with increasing exposure time.

ReNcell VM was immunolabeled for actin to detect potential alterations to cytoskeletal structure in the cells treated with varying rotenone up to 36 h (Fig. 5a). While NPCs appeared more spread with distinguishable actin filaments in control cultures, even after 36 h, an exposure duration–concentration-dependent compromise in cellular morphology was evident in rotenone-exposed cultures. Significant actin reorganization with more protein aggregation at the periphery and depletion in the cytoplasm was noted with rotenone addition. Similarly, the average cellular area of ReNcell VM ( $\sim 1650$  μm<sup>2</sup>) significantly decreased at all rotenone concentrations tested and at every time point (Fig. 5b).

### Biochemical and biomechanical effects of digoxin exposure

A concentration-dependent decrease in ReNcell VM viability was noted after 24 h exposure to range of digoxin concentrations (0.2–50 μM), with  $IC_{50} \approx 0.56 \pm 0.01$  μM (Fig. 2a). The mechanisms by which digoxin induced cellular damage was assessed by quantifying changes in DNA ( $IC_{50} \approx 2.02 \pm 0.09$  μM) and mitochondria ( $IC_{50} \approx 0.94 \pm 0.02$  μM), and intracellular glutathione levels ( $IC_{50} \approx 0.84 \pm 0.02$  μM) (Fig. 2b). Based on these  $IC_{50}$  values, plasma membrane integrity (Live/Dead<sup>®</sup> assay) seems

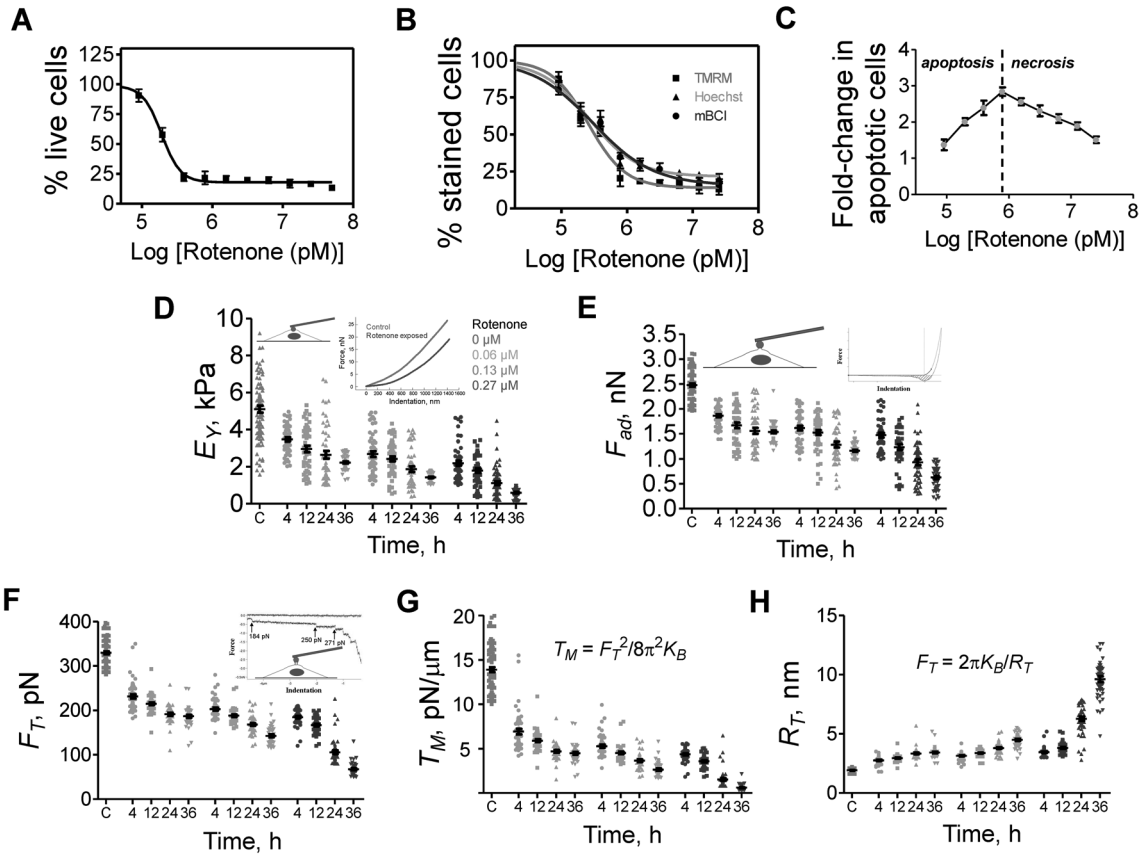


**Fig. 1** ReNCell VM was exposed to a range of rotenone concentrations (0.1–25  $\mu\text{M}$ ) for 24 h. Concentration-dependent cell survival (a), DNA damage, mitochondrial impairment, and changes in intracellular glutathione levels (b), and apoptosis-induced cell death (c) in rotenone-exposed cultures. The transition from apoptosis to necrosis as the mechanism of death is marked for visualization. Biomechanical characteristics such as elastic modulus (d), force of adhesion (e), tether force (f), apparent membrane tension (g), and radius of tether (h) were quantified at various time points (4, 12, 24, and 36 h) and rotenone concentrations (0, 0.06, 0.13, and 0.27  $\mu\text{M}$ ) using AFM, and reported as average  $\pm$  standard error. Representative force-indentation

curves obtained from control and rotenone-exposed cells were shown in the inset in panel D. Elastic modulus was calculated by applying Hertz model to force-indentation curves ( $n \geq 45$  cells/condition) obtained from control and rotenone-exposed cells. Membrane tether forces ( $F_T$ ;  $n \geq 50$  cells/condition), apparent membrane tension ( $T_M \approx F_T^2/8\pi^2 K_B$ ), and tether radius ( $R_T \approx 2\pi K_B/F_T$ ) were measured by retraction of beaded-AFM probe from the cell surface. Here  $K_B$  is the bending modulus,  $\approx 0.1$  pN $\cdot\mu\text{m}$  for lipid layers. Representative adhesive and tether forces obtained from force-indentation curves were shown in the insets in e and f

to be the dominant mechanism by which ReNcell VM is influenced by digoxin ( $p < 0.01$  vs. other mechanisms; Supplementary Figure 3). An increase in the number of apoptotic cells was observed at  $\leq 0.39$   $\mu\text{M}$  digoxin (Fig. 2c), and no changes in SOX2 expression were observed within surviving and undetached ReNcell VM upon digoxin exposure at  $\leq \text{IC}_{50}$  concentrations (Supplementary Figure 1).

Similar to the trends noted for rotenone exposure, significant decreases in  $E_Y$ ,  $F_{adh}$ ,  $F_T$ , and  $T_M$  with concomitant increases in  $R_T$  was noted with increasing digoxin concentration ( $p < 0.001$  vs. controls) and exposure time ( $p < 0.001$  vs. controls) (Fig. 2d–h). At a fixed digoxin concentration, significant differences in the observed properties were noted with increasing exposure duration; similarly, at every time point tested, significant differences in mechanical and physical characteristics were evident with increasing digoxin

concentration. Significant digoxin concentration and exposure time-dependent loss in actin meshwork and cytoskeleton reorganization were evident in ReNcell VM (Fig. 5a). Except for 0.14  $\mu\text{M}$  concentration and 4 h treatment, digoxin exposure significantly compromised the cellular area at all concentrations and time points tested vs. controls (Fig. 5c).

### Biochemical and biomechanical effects of AEA exposure

A concentration-dependent decrease in cell viability with  $\text{IC}_{50} \approx 8 \pm 0.13$   $\mu\text{M}$  was noted (Fig. 3a) upon ReNcell VM exposure to a range of AEA concentrations (0.11–30  $\mu\text{M}$ ). The mechanisms by which AEA influences ReNcell VM was assessed by quantifying changes in intracellular glutathione levels ( $\text{IC}_{50} \approx 6.4 \pm 0.33$   $\mu\text{M}$ ), DNA

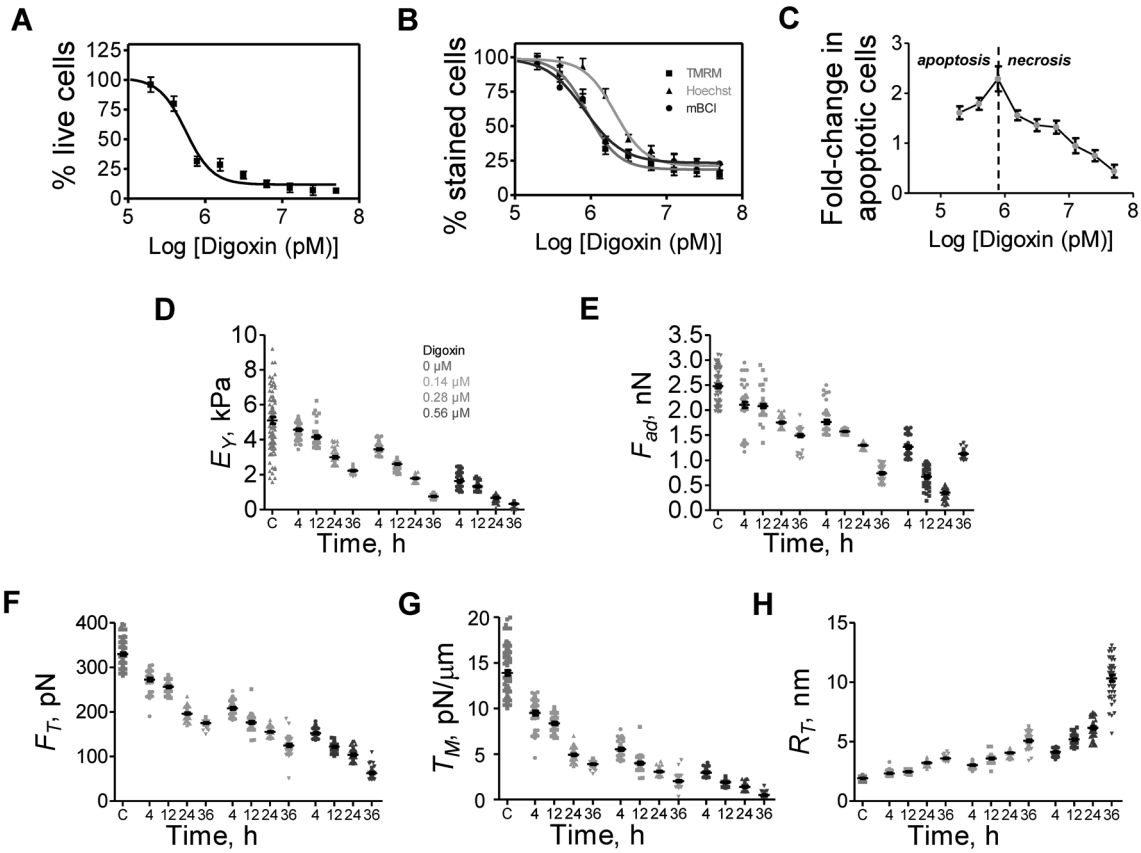


**Fig. 2** ReNcell VM was exposed to a range of digoxin concentrations (0.2–50  $\mu\text{M}$ ) for 24 h. Concentration-dependent cell survival (a), DNA damage, mitochondrial impairment, and changes in intracellular glutathione levels (b), and apoptosis-induced cell death (c) in digoxin-exposed cultures. The transition from apoptosis to necrosis as the mechanism of death is marked for visualization. Biomechanical characteristics such as elastic modulus (d), force of adhesion (e), tether force (f), apparent membrane tension (g), and radius of tether

(h) were quantified at various time points (4, 12, 24, and 36 h) and digoxin concentrations (0, 0.14, 0.28, and 0.56  $\mu\text{M}$ ) using AFM, and reported as average  $\pm$  standard error. Elastic modulus was calculated by applying Hertz model to force-indentation curves ( $n \geq 45$  cells/condition) obtained from control and digoxin-exposed cells. Membrane tether forces ( $F_T$ ;  $n \geq 50$  cells/condition), apparent membrane tension ( $T_M \approx F_T^2/8\pi^2 K_B$ ), and tether radius ( $R_T \approx 2\pi K_B/F_T$ ) were measured by retraction of beaded-AFM probe from the cell surface

damage ( $\text{IC}_{50} \approx 11.4 \pm 0.23 \mu\text{M}$ ), and mitochondrial damage ( $\text{IC}_{50} \approx 4.3 \pm 0.16 \mu\text{M}$ ) (Fig. 3b). Based on these  $\text{IC}_{50}$  values, changes in mitochondrial membrane potential seems to be the dominant mechanism by which AEA affects ReNcell VM ( $p < 0.01$  vs. other mechanisms; Supplementary Figure 3). Apoptosis seems to be dominant mechanism up to 0.48  $\mu\text{M}$  of AEA (Fig. 3c). NPC differentiation was not noted in AEA-exposed cultures, as evident from SOX2 expression in surviving cells (Supplementary Figure 1).

Significant decreases in  $E_\gamma$ ,  $F_{\text{adh}}$ ,  $F_T$ , and  $T_M$  and increase in  $R_T$  over 36 h ( $p < 0.001$  vs. controls) and higher AEA concentrations ( $p < 0.001$  vs. controls) were noted (Fig. 3d–h). At every time point tested, significant compromise in mechanical properties of ReNcell VM was noted with increasing AEA concentrations. Similarly, significant changes in biomechanical characteristics of ReNcell VM were observed with increasing exposure duration at a fixed AEA concentration. AEA exposure led to time and

concentration-dependent upregulation in F-actin degradation and cytoskeleton reorganization (Fig. 5a), and significant compromises in the cell area (Fig. 5d).

### Biochemical and biomechanical effects of chlorpyrifos exposure

When ReNcell VM was treated with chlorpyrifos (0.1–50  $\mu\text{M}$ ), a concentration-dependent decrease in cell viability was observed with  $\text{IC}_{50} \approx 9.9 \pm 0.17 \mu\text{M}$  (Fig. 4a). The subcellular mechanisms of chlorpyrifos toxicity were assessed by quantifying changes in mitochondrial membrane potential ( $\text{IC}_{50} \approx 5.5 \pm 0.23 \mu\text{M}$ ), nucleic DNA damage ( $\text{IC}_{50} \approx 11.6 \pm 0.45 \mu\text{M}$ ), and intracellular glutathione levels ( $\text{IC}_{50} \approx 8.25 \pm 0.25 \mu\text{M}$ ) (Fig. 4b). Based on these  $\text{IC}_{50}$  values, mitochondrial damage seems to be the dominant mechanism by which chlorpyrifos influences a compromise in ReNcell VM health ( $p < 0.01$  vs. other mechanisms;

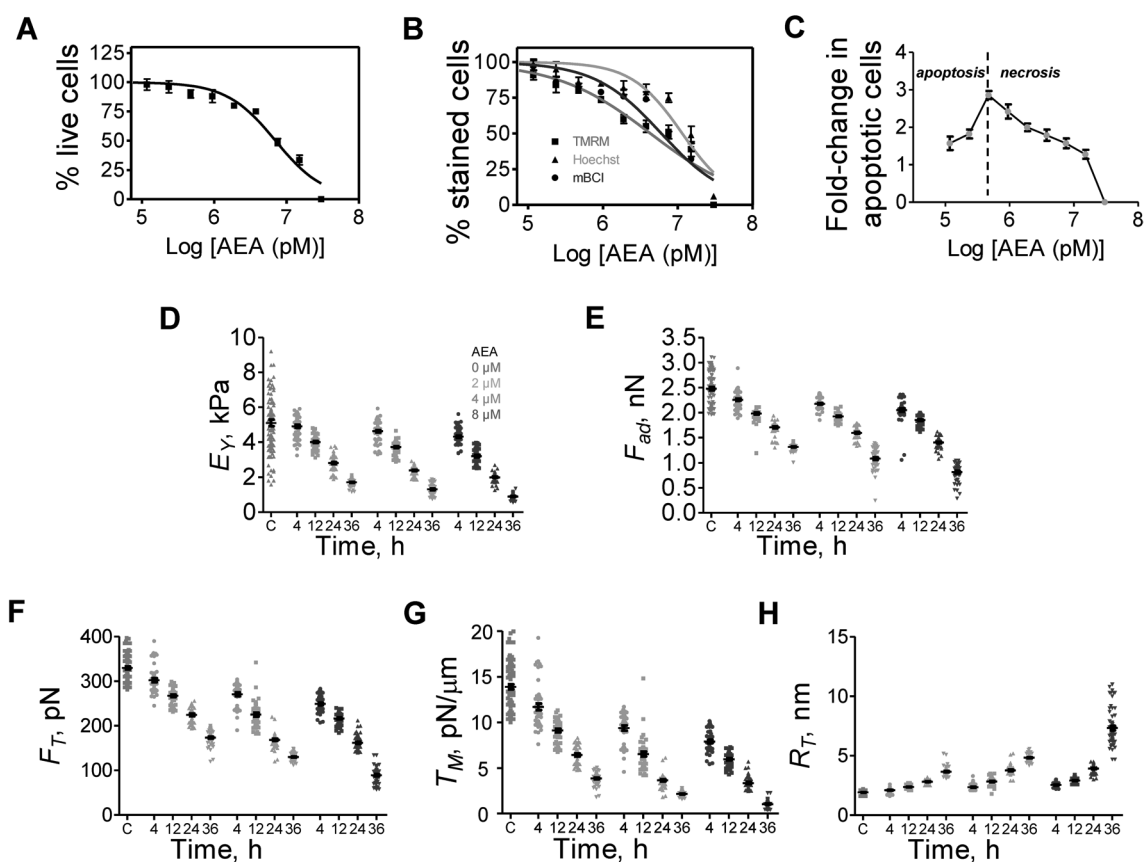


**Fig. 3** ReNCell VM was exposed to a range of AEA concentrations (0.11–30  $\mu\text{M}$ ) for 24 h. Concentration-dependent cell survival (a), DNA damage, mitochondrial impairment, and changes in intracellular glutathione levels (b), and apoptosis-induced cell death (c) in AEA-exposed cultures. The transition from apoptosis to necrosis as the mechanism of death is marked for visualization. Biomechanical characteristics such as elastic modulus (d), force of adhesion (e), tether force (f), apparent membrane tension (g), and radius of tether

(h) were quantified at various time points (4, 12, 24, and 36 h) and AEA concentrations (0, 2, 4, and 8  $\mu\text{M}$ ) using AFM, and reported as average  $\pm$  standard error. Elastic modulus was calculated by applying Hertz model to force-indentation curves ( $n \geq 45$  cells/condition) obtained from control and AEA-exposed cells. Membrane tether forces ( $F_T$ ;  $n \geq 50$  cells/condition), apparent membrane tension ( $T_M \approx F_T^2/8\pi^2 K_B$ ), and tether radius ( $R_T \approx 2\pi K_B/F_T$ ) were measured by retraction of beaded-AFM probe from the cell surface

Supplementary Figure 3). An increase in the number of apoptotic cells was noted up to 0.78  $\mu\text{M}$  chlorpyrifos, after which necrosis might be dominant (Fig. 4c). No changes in SOX2 expression were evident upon chlorpyrifos exposure (Supplementary Figure 1).

A concentration-time-dependent decrease ( $p < 0.001$  vs. controls) in  $E_Y$ ,  $F_{\text{ad}}$ ,  $F_T$ , and  $T_M$  and concomitant increase in  $R_T$  ( $p < 0.001$  vs. controls) of ReNcell VM were observed upon exposure to chlorpyrifos (Fig. 4d–h). At a fixed chlorpyrifos concentration, a significant drop in biophysical and biomechanical characteristics of ReNcell VM was observed with increasing time. Similarly, at every exposure time point tested, a significant decrease in ReNcell VM biomechanics was observed with increasing concentration. Finally, gradual changes in cytoskeleton organization with actin down-regulation (Fig. 5a) and shrinkage of the cell area (Fig. 5e) were observed with increasing chlorpyrifos concentration and exposure time.

## Discussion

Recent studies have demonstrated vulnerability of a developing fetus when it encounters even trace amounts of environmental toxicants which are harmless to most adults (Landrigan and Goldman 2011). The developing CNS is susceptible to damage by exposure to toxicants primarily due to the still immature blood-brain barrier. Since NPCs are among the most sensitive cell types, they are commonly used as model cells to screen compounds for their neurotoxic potential. A few recent studies, including from our group, have evaluated the role of various toxicants (e.g., heavy metals, pharmaceutical compounds, PCBs) on the sensitivity of immortalized and primary NPCs isolated from various species (e.g., murine, human) (Tamm and Ceccatelli 2017; Tasneem et al. 2016). Since insulating NPCs from toxic insult during embryogenesis is crucial not only for proper CNS development, but also during later stages of life, the

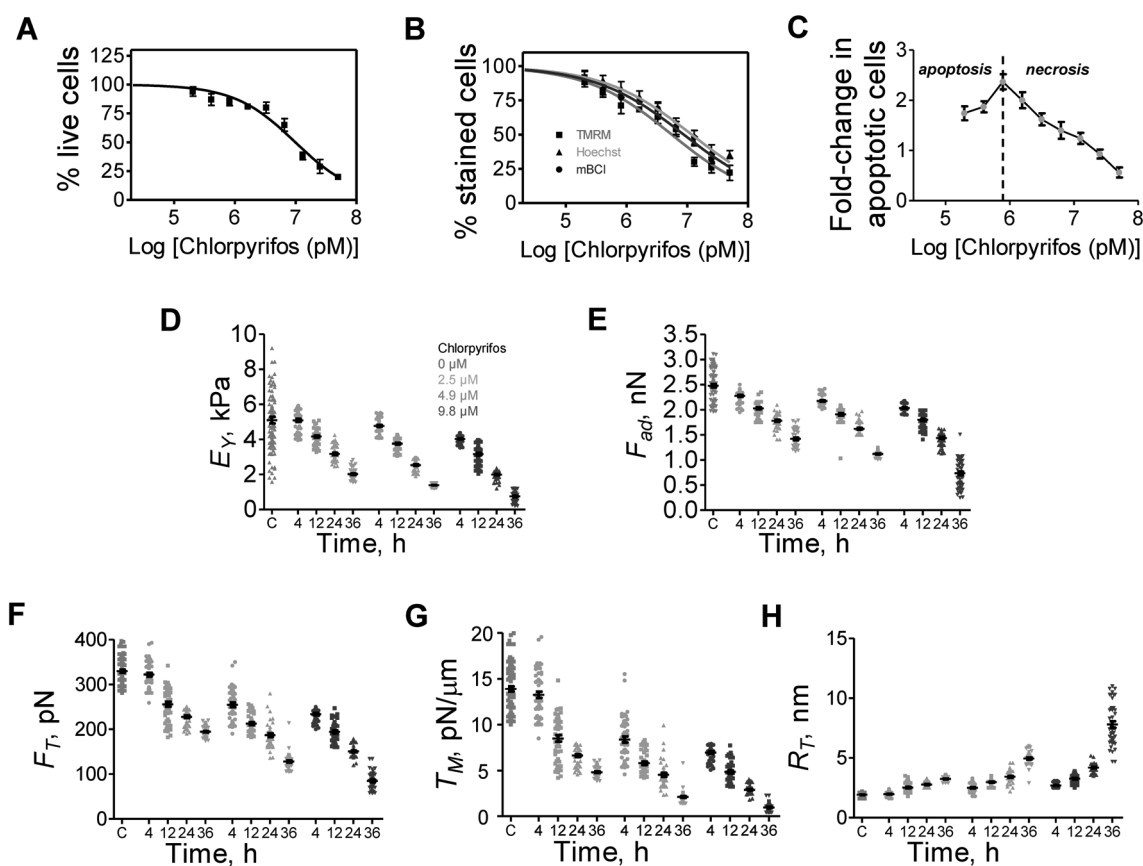


**Fig. 4** ReNCell VM was exposed to a range of chlorpyrifos concentrations (0.1–50  $\mu$ M) for 24 h. Concentration-dependent cell survival (a), DNA damage, mitochondrial impairment, and changes in intracellular glutathione levels (b), and apoptosis-induced cell death (c) in chlorpyrifos-exposed cultures. The transition from apoptosis to necrosis as the mechanism of death is marked for visualization. Biomechanical characteristics such as elastic modulus (d), force of adhesion (e), tether force (f), apparent membrane tension (g), and radius of

tether (h) were quantified at various time points (4, 12, 24, and 36 h) and chlorpyrifos concentrations (0, 2.5, 4.9, and 9.8  $\mu$ M) using AFM, and reported as average  $\pm$  standard error. Elastic modulus was calculated by applying Hertz model to force-indentation curves ( $n \geq 45$  cells/condition) obtained from control and AEA-exposed cells. Membrane tether forces ( $F_T$ ;  $n \geq 50$  cells/condition), apparent membrane tension ( $T_M \approx F_T^2/8\pi^2 K_B$ ), and tether radius ( $R_T \approx 2\pi K_B/F_T$ ) were measured by retraction of beaded-AFM probe from the cell surface

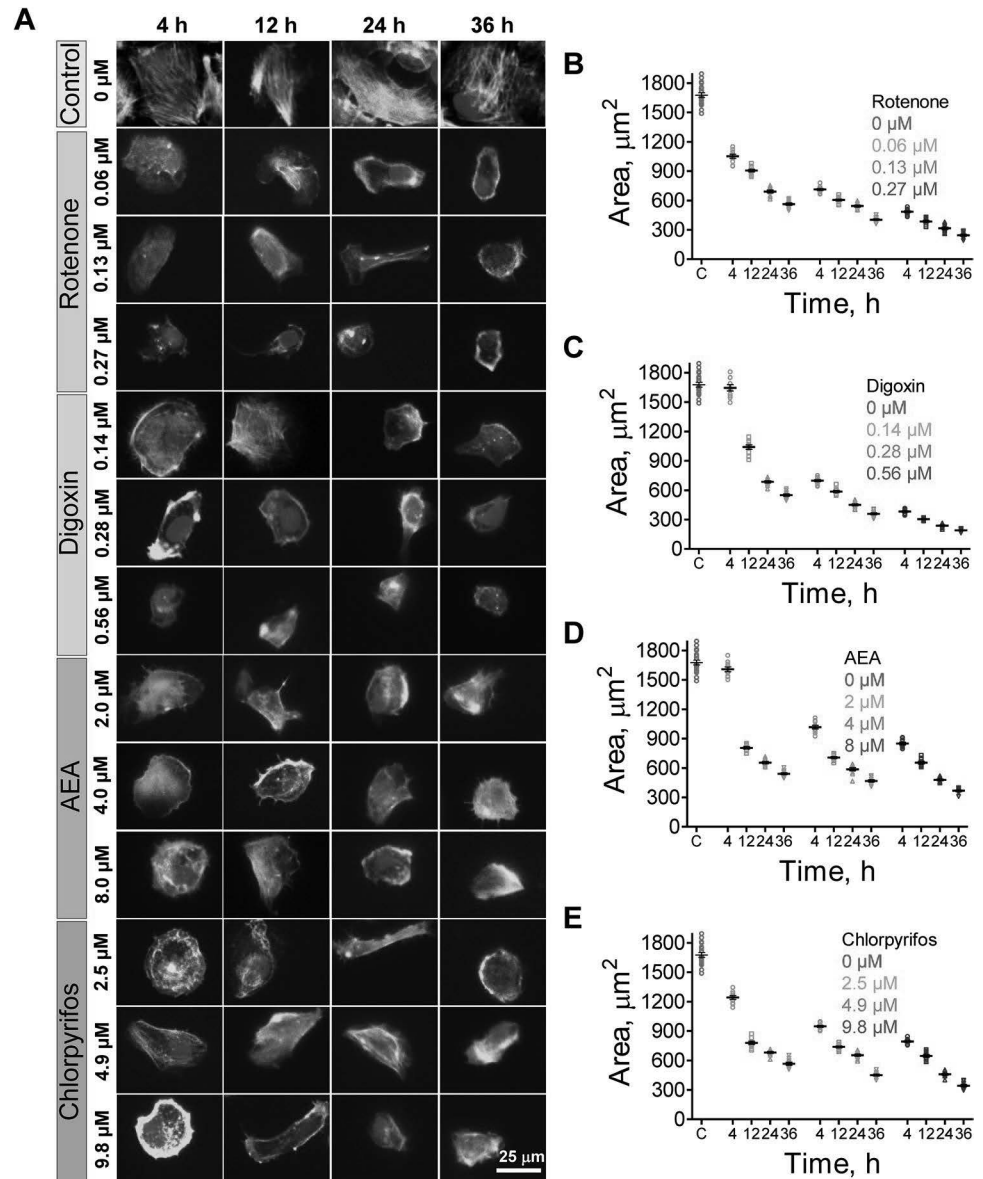
goal of this study is to screen a variety of compounds used in daily lives for their cytotoxic potential on NPCs, evaluate the sub-cellular mechanisms by which these compounds induce damage to these cells, elucidate the biomechanical and biophysical changes in these cells upon toxicant exposure, and finally correlate the biochemical and biophysical changes. To our knowledge, we report here for the first time on the biophysical and biomechanical changes in human NPCs upon exposure to toxic compounds, including the four compounds tested. Specifically, we here show that although most cells survived for more than 24 h at very low dosages of the compounds (e.g.,  $0.25 \times IC_{50}$ ), their mechanical properties were severely compromised even after 4 h of incubation.

Rotenone, a plant-derived product and commonly used as an insecticide, blocks electron flow from NADH to coenzyme Q. Prior studies reported on the  $IC_{50}$  values of rotenone (0.02–200  $\mu$ M) depending on the cell type (Murtaza et al. 2016), and rotenone-induced apoptosis on various

in vitro platforms (Li et al. 2005; Seoposengwe et al. 2013). We observed a concentration-dependent NPC death upon rotenone exposure, and found NPCs to be the most sensitive to mitochondrial damage as reported by others (Gomez et al. 2007). Similar results were observed when neuroblastomas were exposed to rotenone, leading to reduction in intracellular ROS and decreased intracellular glutathione levels, both contributing to apoptosis (Seoposengwe et al. 2013). NPCs exposed to rotenone showed caspase 9/3 independent apoptosis, a time-dependent release of cytochrome c and apoptosis-inducing factor, following mitochondrial depolarization-based increase in ROS generation, leading to apoptosis (Li et al. 2005). Despite such information, the biophysical and biomechanical changes induced by rotenone on NPCs (or other cells) remained unexplored.

Digoxin is one of the most widely used cardiac medications recommended by the American Heart Association, although it does not have a favorable efficacy and safety

**Fig. 5 a** Representative immunofluorescence images of ReN-Cell VM showing morphological changes, i.e., reorganization of F-actin mesh network, in the presence of various toxicants, over 36 h exposure. Cellular area was quantified at various concentrations of rotenone (**b**), digoxin (**c**), AEA (**d**), and chlorpyrifos (**e**), over a 36-h period. Scale bar: 25  $\mu\text{m}$



profile. Various studies have evaluated digoxin's neurotoxic potential (Hoffmann et al. 2010; Svensson et al. 2005) and found that to be toxic to human NPCs but not rat NPCs; similar data was obtained for other cardiac glycosides (Malik et al. 2014). Digoxin was also reported to be toxic to iPSCs, neurons and fetal astrocytes (Svensson et al. 2005). Cells exposed to digoxin showed a distinct morphology which can be correlated to its mechanisms of toxicity. Digoxin was found to have an inhibiting action on neuroblastoma growth in vitro, and on the growth of murine or human neuroblastoma in vivo (Svensson et al. 2005). In agreement with previous studies (Arispe et al. 2008; Gardner et al. 1973), our results have shown a compromise in membrane integrity upon digoxin exposure, leading to dose-dependent cytotoxicity. This specificity of digoxin on cells of CNS origin suggests an urgent need for

in-depth testing of its developmental neurotoxicity (Hoffmann et al. 2010).

Chlorpyrifos is one of the most widely investigated organophosphates for developmental neurotoxicity (Lee et al. 2016), and its regulation and usage remain highly controversial. Despite much work done to evaluate the toxic effects of chlorpyrifos, the underlying mechanism remains unknown, which projects an urgent need for better assays to elucidate the toxic nature of chlorpyrifos (Giordano and Costa 2012; Gohner et al. 2014; Slotkin et al. 2012). The  $\text{IC}_{50}$  value of chlorpyrifos we obtained is in the range of previous studies (0.8–56  $\mu\text{M}$ ) noted in human brain cells (Burke et al. 2017; Eaton et al. 2008). Studies have shown the effects of chlorpyrifos not only during early stages of brain development in murine models, but also in the later stages of brain development. For instance, chlorpyrifos

was shown to induce neurobehavioral abnormalities during second and third postnatal weeks in rats, which corresponds to human neonatal stages (Bjorling-Poulsen et al. 2008). Chronic exposure of chlorpyrifos has been linked to neurocognitive and neurobehavioral deficits, with glial cells more susceptible than neurons (Bal-Price et al. 2010). It has been reported that oxidative stress, inflammation, and/or irreversible neuropathies might be the mechanisms involved in such chronic exposure. Experimental studies utilizing rodent models showed that pre- and post-natal exposure of chlorpyrifos leads to alternation in many cellular processes, including proliferation and DNA replication (Giordano and Costa 2012). Various studies have shown the differential effect of chlorpyrifos exposure; *in vitro* models suggested an increase in neuronal apoptotic process and a decrease in glial proliferation (Giordano and Costa 2012; Gohner et al. 2014). In our study, mitochondrial impairment and glutathione depletion by oxidative stress are the main mechanisms of chlorpyrifos-induced cytotoxicity along with apoptosis, in agreement with previous studies (Salama et al. 2014; Yamada et al. 2017).

In recent years there has been a spike in the use of recreational drugs and other cannabis. The biologically active compound of cannabis,  $\Delta^9$ -tetrahydrocannabinol, affects by binding to cannabinoid receptors. The long-term motor defects in the offspring and involvement of these compounds in neural differentiation was reported (Contassot et al. 2004a, b). The use (abuse) of these compounds during pregnancy poses an existential threat to the developing fetus. However, lack of pertinent data dictates an urgent need to elucidate the mechanisms underlying the cytotoxic potential of AEA (Contassot et al. 2004a, b). Most of these recreational drugs are cationic lipophilic molecules which can readily cross placenta and blood–brain barrier to influence amniotic fluid and fetal tissues (Movsesyan et al. 2004). On the other hand, some studies have shown the neuroprotective nature of endocannabinoids, both *in vivo* and *in vitro*. AEA offered protective biological effects after brain injury and in neuronal cultures mimicking ischemic conditions, making them a valuable target for drug discovery. Our results show a dose-dependent AEA-induced cell death in NPC cultures, with mitochondrial damage driving the mechanism of cell sensitivity to AEA below  $IC_{50}$  levels, followed by intracellular glutathione levels. Apart from their neuroprotective effects, studies have shown the cytotoxic effects of AEA in cortical and hippocampal neuron cultures, mainly mediated by caspase-3 dependent apoptosis and ROS generation (Cernak et al. 2004). Using YO-PRO<sup>®</sup>-1 assay which only stains for apoptotic cells, we observed an increase in apoptotic cells up to a certain concentration for each toxicant tested, followed by a decrease in cells staining positive for apoptotic marker, although cell death continued to monotonically rise with increasing toxicant concentration. While the crosstalk

between signaling networks involved in the mechanisms of cell death (apoptosis vs. necrosis) could not be completely decoupled, numerous studies attest to the role of apoptosis as the dominant mechanism at low concentrations and necrosis taking over that role at higher dosages of a variety of toxicants (Messner et al. 2012; O'Brien et al. 2000; Yeung et al. 1999; Zaucke et al. 1998), similar to that noted in our studies. Exposure of cigarette smoke condensate led to activation of p53-mediated activation of apoptotic signaling at low concentrations and interruption in apoptotic signaling leading to necrosis at higher concentrations (Messner et al. 2012). Similarly, lower taxol concentrations led to blocking of mitosis and onset of apoptosis whereas higher levels led to microtubule polymerization and necrosis induction (Yeung et al. 1999). A hallmark of necrosis is the loss of membrane integrity (Li and Zhou 2015; Sachet et al. 2017). Our AFM analysis showed that apparent membrane tension decreased with both increasing concentration and exposure time (Figs. 1g, 2g, 3g, 4g), indicating loss of membrane integrity and induction of necrosis.

To our knowledge, there is no existing literature on the characterization of cellular biomechanics of human NPCs, nor the effect of these four compounds on biomechanical characteristics of any cell types. Therefore, our study addresses a critical gap in literature and establishes a baseline for biochemical and biophysical changes in NPCs in the presence of toxicants. Our results showed a significant effect of toxicant exposure on cellular elasticity, adhesion, tether forces, radius of tether, and membrane tension, compared to untreated NPCs. The elastic modulus of NPCs decreased by ~80% upon exposure to 0.27  $\mu$ M of rotenone for 24 h. In select cases, prolonged exposure of lower toxicant concentrations showed similar effects on biomechanical properties as short-term exposure at higher concentrations, suggesting the need to extend the extent of toxicity testing beyond  $IC_{50}$  values. Two-way ANOVA revealed significant primary effects of concentration ( $p < 0.001$ ), exposure time ( $p < 0.001$ ), and interaction between concentration and exposure time ( $p < 0.001$ ) on NPCs for all the compounds tested.

We correlated the change in Young's modulus to cell death measured from the most sensitive mechanistic assay (e.g., mitochondrial impairment), pooled for all four different neurotoxicants (Fig. 6). A strong negative correlation ( $R^2 = 0.92$ ) between the normalized elastic modulus (to controls) of surviving cells and the percentage of living cells in that environment was noted, suggesting that (a) the health of organelles in a toxic environment strongly influences cell mechanics, (b) cell biomechanics could also be correlated to biochemical outcomes, in addition to biophysical changes, and (c) biomechanical characteristics (modulus, tether forces, adhesion) are key markers and predictors of neurotoxicity. In studies exploring role of silver nanoparticles on human embryonic kidney cells, a similar strong

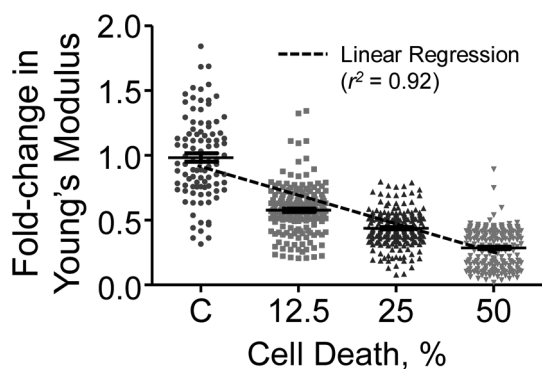


**Fig. 6** Changes in elastic modulus of human NPCs were correlated to compromise in cell death calculated from most sensitive assay upon toxicants exposure. A strong negative correlation ( $R^2=0.92$ ) was noted suggesting that the biomechanical properties can be correlated to sub-cellular mechanism of cell death induced by toxicants. Here C refers to control cultures which did not receive any compounds

negative correlation between DNA damage and factor of viscosity was noted (Jiang et al. 2018). Multivariate logistic regression analysis (Alexopoulos 2010; Kozel et al. 2014) suggested that elastic modulus ( $p < 0.001$ ), adhesion force ( $p < 0.0001$ ), and tether force ( $p < 0.0001$ ) were significant predictors of NPC toxicity. The receiver operating characteristic (ROC) was analyzed to gauge the utility of elastic modulus, adhesion force, and tether force as reliable indicators of NPC health, resulting in the model given by:  $M = 1.672 - 0.033 \times E_Y - 0.109 \times F_{ad} - 0.003 \times F_T$ , where  $E_Y$  (elastic modulus) is in kPa,  $F_{ad}$  (adhesion force) is in nN, and  $F_T$  (tether force) is in pN units. Based on the Akaike information criterion (AIC) calculated from this model (Wang 2013), changes in tether force appears to be the strongest predictor of neurotoxicity.

The time–concentration-dependent decrease in adhesion force upon toxicant exposure suggests an alteration of cell membrane, possibly the modification of surface adhesion molecules. The polysaccharides on cell surface and secreted ECM proteins are primarily responsible for cellular adhesion. Typically, an increase in adhesion force suggests an aggregation of polysaccharides, while a decrease in adhesion force suggests denaturation or detachment of polysaccharides from cell surface. Cell adhesion molecules such as integrins, proteoglycans, selectins, cadherins, oligosaccharides, and immunoglobulins mediate cell–cell and cell–ECM interactions (Müller and Dufrêne 2011). Exposure to heavy metals (e.g., lead, methylmercury) and organic sulfates led to altered expression and function of cell adhesion molecules such as cadherins and IgCAMs (Grunwald 2018). Upon exposure of glyphosate (a herbicide), a concentration-dependent reduction in cell adhesion was observed in MC3T3-E1 cells, via blocking of RGD-specific integrin (Szekacs et al. 2018). Inhibiting fibronectin–integrin

binding leads to a strong decrease in adhesion force of primary gastrulating cells as detected by AFM analysis (Puech et al. 2005). Adhesion force is an encouraging biomarker for changes in cell surface due to inflammation or differentiation (Pi et al. 2014; Xing et al. 2011). Our observations on changes in adhesion forces of NPCs are in line with reports on human aortic endothelial cells exposed to diesel exhaust particles (Wu et al. 2012).

Various techniques (e.g., micropipette aspiration, optical-tweezers, magnetic twisting cytometry, microfluidics, AFM) have been developed to study cell biomechanics, to understand how cells perceive transformations and perturbation due to mechanical forces. For instance, optical tweezer analysis of erythrocytes and leukemic cells exposed to doxorubicin showed a decrease in cell modulus, demonstrating the need for biomechanical assays to screen the toxic concentration of drugs and prevent the risk of vascular complications due to high dosages (Fraczkowska et al. 2018). However, the unique capabilities of AFM such as non-invasive characterization, measurements under physiological conditions, precise control on the magnitude and frequency of the applied forces, and high spatial control, makes it the most suitable technique to image and mechanically characterize either fixed or live cells or tissues.

From the retraction profile of force–indentation curve, we quantified the forces involved in individual and multiple membrane tethers on NPCs in the presence and absence of the compounds (50–400 pN). Our results are in the range of tether forces measured using techniques such as AFM or optical tweezers, for a variety of different cells and vesicles (Pontes et al. 2011; Sun et al. 2005). Toxicant-exposed NPCs showed higher values of tether radius as compared to control cells, indicating a weak connection between cytoskeleton and plasma membrane upon toxicant exposure. The average apparent membrane tension decreased from 13.9 nN/ $\mu\text{m}$  in control cells to 0.5 nN/ $\mu\text{m}$  upon exposure to 0.56  $\mu\text{M}$  digoxin. Such compromise in apparent membrane tension follows the similar patterns observed with cellular stiffness and cellular adhesion. However, changes in adhesive forces, tether forces, or membrane tension would have less effect on cell elastic modulus compared to alterations in actin cytoskeleton.

Cell shape is maintained by the cortical tension, cell–matrix adhesion, cell–cell contact, and the microenvironment. Various developmental stages require changes in cell shape which contribute to morphogenetic processes. CNS diseases (e.g., Parkinson’s, Alzheimer’s) and disorders (e.g., neural tube defects) have been shown to be associated with the rearrangement of the cytoskeleton (May-Simera and Liu 2013). Therefore, the significant time–concentration-dependent changes in NPC cytoskeleton upon toxicant exposure is of interest as it could lead to developmental defects in the short term (changes in NPC migration, differentiation)

and neurodegenerative diseases in the long term. Although genetic and epigenetic changes could be expected in NPCs exposed to toxicants, it was not the primary goal of this study and therefore will be investigated in future studies.

In conclusion, we investigated and correlated the cytotoxic, biophysical and biomechanical aspects of a variety of classes of compounds on human NPCs. We highlighted the role of cell biomechanics as a crucial marker and predictor of developmental neurotoxicity by demonstrating a compromise in cellular mechanics upon exposure to four different classes of toxicants. A negative linear correlation between the levels of cell death in vitro upon toxicant exposure and the intrinsic changes in cell elastic modulus was noted. We propose the term mechanotoxicology to ascribe cellular mechanics as an important toxicity endpoint and validated the utility of developmentally relevant human NPCs as an appropriate cell model for compound screening. We also elucidated the underlying mechanisms of cell death and deterioration of cell health associated with toxicant exposure. Our current studies are geared towards investigating genetic changes corresponding to perturbation of cellular mechanics, as well as investigating the effects of these compounds on NPCs differentiation.

**Acknowledgements** The authors acknowledge help from Soo-Yeon Kang with cell passaging and high-content imaging equipment. This work was partially supported by funds from National Institutes of Health (NIEHS R01ES025779) to C.K. and M.Y.L., National Science Foundation (CBET, Award # 1337859) to C.K., and Graduate Student Research Award to G.M from Cleveland State University.

## Compliance with ethical standards

**Conflict of interest** The authors declare that they have no conflict of interest.

**Ethical standards** The manuscript does not contain clinical studies or patient data.

## References

- Alexopoulos EC (2010) Introduction to multivariate regression analysis. *Hippokratia* 14(Suppl 1):23–28
- Angely C, Nguyen NM, Planus E et al (2017) Exposure to Bordetella pertussis adenylate cyclase toxin affects integrin-mediated adhesion and mechanics in alveolar epithelial cells. *Biol Cell* 109(8):293–311
- Arisepe N, Diaz JC, Simakova O, Pollard HB (2008) Heart failure drug digitoxin induces calcium uptake into cells by forming transmembrane calcium channels. *Proc Natl Acad Sci USA* 105(7):2610–2615
- Bal-Price AK, Hogberg HT, Buzanska L, Lenas P, van Vliet E, Hartung T (2010) In vitro developmental neurotoxicity (DNT) testing: relevant models and endpoints. *Neurotoxicology* 31(5):545–554
- Barnes JM, Przybyla L, Weaver VM (2017) Tissue mechanics regulate brain development, homeostasis and disease. *J Cell Sci* 130(1):71–82
- Bjorling-Poulsen M, Andersen HR, Grandjean P (2008) Potential developmental neurotoxicity of pesticides used in Europe. *Environ Health* 7:50
- Burke RD, Todd SW, Lumsden E et al (2017) Developmental neurotoxicity of the organophosphorus insecticide chlorpyrifos: from clinical findings to preclinical models and potential mechanisms. *J Neurochem* 142(Suppl 2):162–177
- Cernak I, Vink R, Natale J et al (2004) The “dark side” of endocannabinoids: a neurotoxic role for anandamide. *J Cereb Blood Flow Metab* 24:564–578
- Contassot E, Tenan M, Schnuriger V, Pelte MF, Dietrich PY (2004a) Arachidonyl ethanolamide induces apoptosis of uterine cervix cancer cells via aberrantly expressed vanilloid receptor-1. *Gynecol Oncol* 93(1):182–188
- Contassot E, Wilmotte R, Tenan M et al (2004b) Arachidonyl ethanolamide induces apoptosis of human glioma cells through vanilloid receptor-1. *J Neuropathol Exp Neurol* 63(9):956–963
- Diz-Munoz A, Krieg M, Bergert M et al (2010) Control of directed cell migration in vivo by membrane-to-cortex attachment. *PLoS Biol* 8(11):e1000544
- Diz-Munoz A, Fletcher DA, Weiner OD (2013) Use the force: membrane tension as an organizer of cell shape and motility. *Trends Cell Biol* 23(2):47–53
- Dubovicky M, Kovacovsky P, Ujhazy E, Navarova J, Brucknerova I, Mach M (2008) Evaluation of developmental neurotoxicity: some important issues focused on neurobehavioral development. *Interdiscip Toxicol* 1(3–4):206–210
- Eaton DL, Daroff RB, Autrup H et al (2008) Review of the toxicology of chlorpyrifos with an emphasis on human exposure and neurodevelopment. *Crit Rev Toxicol* 38:1–125
- Ebert AD, Liang P, Wu JC (2012) Induced pluripotent stem cells as a disease modeling and drug screening platform. *J Cardiovasc Pharmacol* 60(4):408–416
- Fraczkowska K, Bacia M, Przybylo M et al (2018) Alterations of biomechanics in cancer and normal cells induced by doxorubicin. *Biomed Pharmacother* 97:1195–1203
- Franze K (2013) The mechanical control of nervous system development. *Development* 140(15):3069–3077
- Gardner JD, Kilno DR, Swartz TJ, Butler VP (1973) Effects of digoxin-specific antibodies on accumulation and binding of digoxin by human erythrocytes. *J Clin Invest* 52:1820–1833
- Gavara N, Chadwick RS (2012) Determination of the elastic moduli of thin samples and adherent cells using conical atomic force microscope tips. *Nat Nanotechnol* 7(11):733–736
- Giordano G, Costa LG (2012) Developmental neurotoxicity: some old and new issues. *ISRN Toxicol* 2012:814795
- Gohner C, Svensson-Arvelund J, Pfarrer C et al (2014) The placenta in toxicology. Part IV: battery of toxicological test systems based on human placenta. *Toxicol Pathol* 42(2):345–351
- Gomez C, Bandez MJ, Navarro A (2007) Pesticides and impairment of mitochondrial function in relation with the parkinsonian syndrome. *Front Biosci* 12:1079–1093
- Grunwald GB (2018) Cell adhesion molecules as targets of developmental toxicants. In: McQueen CA (ed) *Comprehensive toxicology*, vol 5, 3rd edn. Elsevier Science, United Kingdom, pp 202–215
- Hochmuth RM, Shao JY, Dai J, Sheetz MP (1996) Deformation and flow of membrane into tethers extracted from neuronal growth cones. *Biophys J* 70:358–369
- Hoffmann S, Kinsner-Ovaskainen A, Prieto P, Mangelsdorf I, Bieler C, Cole T (2010) Acute oral toxicity: variability, reliability, relevance and interspecies comparison of rodent LD50 data from literature surveyed for the ACuteTox project. *Regul Toxicol Pharmacol* 58(3):395–407

- Jiang X, Lu C, Tang M et al (2018) Nanotoxicity of silver nanoparticles on HEK293T cells: a combined study using biomechanical and biological techniques. *ACS Omega* 3(6):6770–6778
- Joshi J, Mahajan G, Kothapalli CR (2018a) Three-dimensional collagenous niche and azacytidine selectively promote time-dependent cardiomyogenesis from human bone marrow-derived MSC spheroids. *Biotechnol Bioeng* 115(8):2013–2026
- Joshi P, Datar A, Yu KN, Kang SY, Lee MY (2018b) High-content imaging assays on a miniaturized 3D cell culture platform. *Toxicol In Vitro* 50:147–159
- Kim KS, Cho CH, Park EK, Jung MH, Yoon KS, Park HK (2012) AFM-detected apoptotic changes in morphology and biophysical property caused by paclitaxel in Ishikawa and HeLa cells. *PLoS One* 7(1):e30066
- Kolahi KS, Mofrad MR (2010) Mechanotransduction: a major regulator of homeostasis and development. *Wiley Interdiscip Rev Syst Biol Med* 2(6):625–639
- Kozel BA, Su CT, Danback JR et al (2014) Biomechanical properties of the skin in cutis laxa. *J Invest Dermatol* 134(11):2836–2838
- Ladran I, Tran N, Topol A, Brennand KJ (2013) Neural stem and progenitor cells in health and disease. *Wiley Interdiscip Rev Syst Biol Med* 5(6):701–715
- Landrigan PJ, Goldman LR (2011) Children’s vulnerability to toxic chemicals: a challenge and opportunity to strengthen health and environmental policy. *Health Aff (Millwood)* 30(5):842–850
- Lee YS, Lewis JA, Ippolito DL et al (2016) Repeated exposure to neurotoxic levels of chlorpyrifos alters hippocampal expression of neurotrophins and neuropeptides. *Toxicology* 340:53–62
- Li Z, Zhou Z (2015) How are necrotic cells recognized by their predators? *Worm* 5(1):e1120400
- Li J, Spletter ML, Johnson DA, Wright LS, Svendsen CN, Johnson JA (2005) Rotenone-induced caspase 9/3-independent and -dependent cell death in undifferentiated and differentiated human neural stem cells. *J Neurochem* 92(3):462–476
- Li QS, Lee GY, Ong CN, Lim CT (2008) AFM indentation study of breast cancer cells. *Biochem Biophys Res Commun* 374(4):609–613
- Liang X, Shi X, Ostrovidov S, Wu H, Nakajima K (2016) Probing stem cell differentiation using atomic force microscopy. *Appl Surf Sci* 366:254–259
- Lins MP, Silva ECO, Silva GR et al (2018) Association between biomechanical alterations and migratory ability of semaphorin-3A-treated thymocytes. *Biochim Biophys Acta* 1862(4):816–824
- Liu YX, Karsai A, Anderson DS et al (2015) Single-cell mechanics provides an effective means to probe in vivo interactions between alveolar macrophages and silver nanoparticles. *J Phys Chem B* 119(49):15118–15129
- Malik N, Efthymiou AG, Mather K et al (2014) Compounds with species and cell type specific toxicity identified in a 2000 compound drug screen of neural stem cells and rat mixed cortical neurons. *Neurotoxicology* 45:192–200
- May-Simera H, Liu C (2013) Neuronal polarity and neurological disorders. *J Neurol Transl Neurosci* 2(1):1026
- Messner B, Frotschnig S, Steinacher-Nigisch A et al (2012) Apoptosis and necrosis: two different outcomes of cigarette smoke condensate-induced endothelial cell death. *Cell Death Dis* 3:e424
- Movsesyan VA, Stoica BA, Yakovlev AG et al (2004) Anandamide-induced cell death in primary neuronal cultures: role of calpain and caspase pathways. *Cell Death Differ* 11(10):1121–1132
- Müller DJ, Dufrêne YF (2011) Force nanoscopy of living cells. *Curr Biol* 21(6):R212–R216
- Murtaza M, Shan J, Matigian N et al (2016) Rotenone susceptibility phenotype in olfactory derived patient cells as a model of idiopathic Parkinson’s disease. *PLoS One* 11(4):e0154544
- O’Brien T, Babcock G, Cornelius J et al (2000) A comparison of apoptosis and necrosis induced by hepatotoxins in HepG2 cells. *Toxicol Appl Pharmacol* 164(3):280–290
- Pastrana HF, Cartagena-Rivera AX, Raman A, Ávila A (2019) Evaluation of the elastic Young’s modulus and cytotoxicity variations in fibroblasts exposed to carbon-based nanomaterials. *J Nanobiotechnology* 17(1):32
- Pi J, Li T, Liu J et al (2014) Detection of lipopolysaccharide induced inflammatory responses in RAW264.7 macrophages using atomic force microscope. *Micron* 65:1–9
- Pillariseti A, Desai JP, Ladjal H, Schiffmacher A, Ferreira A, Keefer CL (2011) Mechanical phenotyping of mouse embryonic stem cells: increase in stiffness with differentiation. *Cell Repogr* 13(4):371–380
- Pontes B, Viana NB, Salgado LT, Farina M, Moura Neto V, Nussenzveig HM (2011) Cell cytoskeleton and tether extraction. *Biophys J* 101(1):43–52
- Puech PH, Taubenberger A, Ulrich F, Krieg M, Muller DJ, Heisenberg CP (2005) Measuring cell adhesion forces of primary gastrulating cells from zebrafish using atomic force microscopy. *J Cell Sci* 118(18):4199–4206
- Qiu H, Zhu Y, Sun Z et al (2010) Short communication: vascular smooth muscle cell stiffness as a mechanism for increased aortic stiffness with aging. *Circ Res* 107(5):615–619
- Rammensee S, Kang MS, Georgiou K, Kumar S, Schaffer DV (2017) Dynamics of mechanosensitive neural stem cell differentiation. *Stem Cells* 35(2):497–506
- Ross EJ, Graham DL, Money KM, Stanwood GD (2015) Developmental consequences of fetal exposure to drugs: what we know and what we still must learn. *Neuropsychopharmacology* 40(1):61–87
- Sachet M, Liang YY, Oehler R (2017) The immune response to secondary necrotic cells. *Apoptosis* 22(10):1189–1204
- Salama M, El-Morsy D, El-Gamal M, Shabka O, Mohamed WM (2014) Mitochondrial complex I inhibition as a possible mechanism of chlorpyrifos induced neurotoxicity. *Ann Neurosci* 21(3):85–89
- Seoposengwe K, van Tonder JJ, Steenkamp V (2013) In vitro neuroprotective potential of four medicinal plants against rotenone-induced toxicity in SH-SY5Y neuroblastoma cells. *BMC Complement Altern Med* 13:353
- Slotkin TA, Card J, Seidler FJ (2012) Chlorpyrifos developmental neurotoxicity: interaction with glucocorticoids in PC12 cells. *Neurotoxicol Teratol* 34(5):505–512
- Sun M, Graham JS, Hegedus B et al (2005) Multiple membrane tethers probed by atomic force microscopy. *Biophys J* 89(6):4320–4329
- Svensson A, Azarbayjani F, Bäckman U, Matsumoto T, Christofferson R (2005) Digoxin inhibits neuroblastoma tumor growth in mice. *Anticancer Res* 25:207–212
- Szekacs I, Farkas E, Gemes BL, Takacs E, Szekacs A, Horvath R (2018) Integrin targeting of glyphosate and its cell adhesion modulation effects on osteoblastic MC3T3-E1 cells revealed by label-free optical biosensing. *Sci Rep* 8(1):17401
- Tamm C, Ceccatelli S (2017) Mechanistic insight into neurotoxicity induced by developmental insults. *Biochem Biophys Res Commun* 482(3):408–418
- Tasneem S, Farrell K, Lee MY, Kothapalli CR (2016) Sensitivity of neural stem cell survival, differentiation and neurite outgrowth within 3D hydrogels to environmental heavy metals. *Toxicol Lett* 242:9–22
- Wang B (2013) Variable selection in ROC regression. *Comput Math Methods Med* 2013:436493
- Wozniak MA, Chen CS (2009) Mechanotransduction in development: a growing role for contractility. *Nat Rev Mol Cell Biol* 10(1):34–43
- Wu Y, Yu T, Gilbertson TA, Zhou A, Xu H, Nguyen KT (2012) Biophysical assessment of single cell cytotoxicity: diesel exhaust particle-treated human aortic endothelial cells. *PLoS One* 7(5):e36885

- Xing F, Wang J, Hu M, Yu Y, Chen G, Liu J (2011) Comparison of immature and mature bone marrow-derived dendritic cells by atomic force microscopy. *Nanoscale Res Lett* 6(1):455
- Xu W, Lakshman N, Morshead CM (2017) Building a central nervous system: the neural stem cell lineage revealed. *Neurogenesis (Austin)* 4(1):e1300037
- Yamada S, Kubo Y, Yamazaki D, Sekino Y, Kanda Y (2017) Chlorpyrifos inhibits neural induction via Mfn1-mediated mitochondrial dysfunction in human induced pluripotent stem cells. *Sci Rep* 7:40925
- Yeung TK, Germond C, Chen X, Wang Z (1999) The mode of action of taxol: apoptosis at low concentration and necrosis at high concentration. *Biochem Biophys Res Commun* 263(2):398–404
- Yim EK, Darling EM, Kulangara K, Guilak F, Leong KW (2010) Nanotopography-induced changes in focal adhesions, cytoskeletal organization, and mechanical properties of human mesenchymal stem cells. *Biomaterials* 31(6):1299–1306
- Yokokawa M, Takeyasu K, Yoshimura SH (2008) Mechanical properties of plasma membrane and nuclear envelope measured by scanning probe microscope. *J Microsc* 232(1):82–90
- Zaucke F, Zöltzer H, Krug HF (1998) Dose-dependent induction of apoptosis or necrosis in human cells by organotin compounds. *Fresenius J Anal Chem* 361(4):386–392

**Publisher's Note** Springer Nature remains neutral with regard to jurisdictional claims in published maps and institutional affiliations.